Published in final edited form as:
Langmuir. 2009 June 16; 25(12): 7084–7089. doi:10.1021/la900149v.

Understanding Factors Affecting Alignment of Self-Assembling Nanofibers Patterned by Sonication-Assisted Solution Embossing

Albert M. Hung[1] and **Samuel I. Stupp**[*,1,2,3]

1*Department of Materials Science and Engineering, Northwestern University, 2220 Campus Drive, Evanston, Illinois 60208−3108*

2*Department of Chemistry, Northwestern University, 2220 Campus Drive, Evanston, Illinois 60208−3108*

3*Feinberg School of Medicine, Northwestern University, 2220 Campus Drive, Evanston, Illinois 60208−3108*

Abstract

We recently reported simultaneous self-assembly, alignment, and patterning of peptide amphiphile (PA) nanofibers over large areas by a soft lithographic technique termed sonication-assisted solution embossing (SASE). The present work examines the effect of ultrasonication, channel width, and nanofiber persistence length λ on the degree of alignment of nanofibers patterned by SASE. Polarized transmission and reflection infrared spectroscopy are used to establish a figure of merit for comparing nanofiber alignment based on a model of the supramolecular structures being composed of oriented β-sheets. The aligned nanostructures show orientation parameters of up to 0.4, and estimates of λ the persistence length from AFM images range from 2.0 to 11 μm depending on the chemical structure of molecules used. The data suggest that stiffer nanofibers, defined as those with longer persistence lengths, may actually align less well due to increased difficulty in cleaving them during the alignment process. Alignment can be enhanced with the addition of ultrasonic agitation and confinement of the self-assembled structures within channels around 400 nm in width.

Introduction

Self-assembly has proven to be a viable strategy for the bottom-up fabrication of complex and useful nanostructures.[1-4] However, the functionality of self-assembled nanostructures will often require controlling their placement and orientation over macroscopic length scales.[5-8] Toward this end, physical patterning of micrometer and submicrometer features may be a useful strategy. If these features induce a specific orientation locally, repeating the features could extend short range order over large areas. Replicating long range order in this manner may amplify useful anisotropic properties that are commonly not accessible due to local disorder. Increasing the degree of order in self-assembling systems also improves their functional specificity.

Discrete, one-dimensional supramolecular nanostructures are particularly interesting for the anisotropic properties inherent in their shape.[6, 9] The ability to control the orientation of such structures would be useful but is difficult given their poor mobility in non-solvated states as a

*E-mail: E-mail: s-stupp@northwestern.edu.

Supporting Information **Available:** Experiment methods for substrate preparation; detailed derivation of orientation model equations; additional polarized transmission IR spectra of solution embossed PA nanofibers and list of vibrational assignments. This material is available free of charge via the Internet at http://pubs.acs.org.

result of their large mass. We recently succeeded in creating large-area, aligned patterns of self-assembled nanofibers of peptide amphiphile (PA) molecules by sonication-assisted solution embossing (SASE).[10] This soft lithographic technique involved assembling the nanofibers from aqueous solution within confining sub-micron channels while under the influence of ultrasonic agitation. Self-assembly was triggered by solvent evaporation, and the nanofibers were forced by steric repulsion in confined spaces to orient parallel to the channel direction. Unlike other alignment techniques,[11-16] SASE is a parallel process that is not limited to creating uniaxially aligned patterns but can be employed to guide nanofibers around turns and through complex paths. This method may also be applicable to a wide range of supramolecular systems.

The supramolecular PA nanofibers are of interest given their bioactive or biomimetic structures and may be useful for a number of applications including angiogenesis, spinal cord injury repair, and templating of inorganic crystals.[17-21] Alignment of these nanofibers enables more in-depth studies of the nature of their interactions with ions, molecules, and cells. Preliminary work suggests that even weak orientation of the nanofibers can impact neural cell morphology. Measuring the alignment of nanofibers patterned by SASE and understanding the mechanism of reorientation is thus important not only for optimizing the patterning process but to control and study interactions of the nanofibers with their environment.

The naturally occurring supramolecular actin fibrils in the cell cytoskeleton are useful to consider as an analogous system when studying the mechanism of PA nanofiber alignment. Actin fibrils have a calculated persistence length of 4−17 μm[22] and have been aligned by confinement within micrometer-scale channels.[23, 24] However, the channel template is not removed as it is in our methodology, which would allow use of the patterned nanofibers in subsequent experiments with fewer confounding effects. In addition, with SASE it may be possible to tune the order parameter by modification of the ultrasonication step, offering a powerful amount of flexibility. Both methods use steric confinement to align one-dimensional nanostructures and are believed to be more effective when the width of the confining channel is smaller than the persistence length λ of the fibers.[10, 23, 24] A determination of λ for PA nanofibers could provide more insight into the possible limits for alignment of nanofibers patterned by SASE. A number of methods have been used to measure λ of one-dimensional supramolecular nanostructures including live monitoring of shape fluctuations, direct mechanical bending, and small-angle neutron scattering,[25-28] although all of them make numerous assumptions or present significant experimental roadblocks. The simplest method for measuring λ is shape analysis of dried nanofibers imaged by atomic force microscopy (AFM) or scanning electron microscopy (SEM).[29-32] We use this method to estimate an apparent value of λ for two different PA nanofibers.

Recent investigations of neat nanofiber films by transmission and reflectance infrared (IR) spectroscopy support the model of the nanofiber as containing internal β-sheet structures aligned along the nanofiber axis.[33-36] Assuming this structural model is valid, alignment of the nanofibers can be probed by polarized transmission infrared (IR) and polarization modulation–infrared reflection–absorption spectroscopy (PM–IRRAS), methods that provide information on molecular orientation.[37-40] In the present work, we use IR spectroscopy to measure the degree of order in films of nanofibers patterned and aligned by SASE. In conjunction with data on persistence length we discuss what factors can affect or improve alignment in these self-assembling systems.

Materials and Methods

The chemical structure of PA molecules **1** and **2** employed in this study are given in Figure 1. Solid-phase synthesis of **1** and **2** have been reported previously.[17, 18, 33, 41] Optical

diffraction gratings (Edmund Industrial Optics) with groove densities of 1200, 2400 and 3600 lines/mm (833 nm, 416 nm, and 278 nm period, respectively) were used as master molds for casting line patterned PDMS stamps. These stamps were employed to create uniaxially aligned patterns of nanofibers of **1** and **2** by SASE. The procedure for casting the stamps, cleaning the substrates in piranha solution, and patterning the nanofibers was detailed previously.[10] Unpatterned samples were made by drop-casting a 0.01 wt% solution of PA onto a piranha cleaned silicon wafer and allowing it to slowly dry over the course of an hour. Samples prepared for polarized transmission FTIR were patterned on piranha-cleaned undoped (111) silicon (n-type, resistivity: 1500 Ωcm, University Wafer). A Thermo Nicolet Nexus 870 FTIR spectrometer was set up in transmission mode with a polarizer in the beam path ahead of the sample. FTIR spectra of the samples were collected for polarization angles ranging from 0° to 90° relative to the grating line direction. Samples made on thin film metal substrates (see supporting information) were studied by PM-IRRAS using the same instrument in grazing-incidence reflection mode with an attached tabletop optics module. Images of unpatterned and SASE patterned nanofibers were acquired on a JEOL 5200 AFM operating in tapping mode or on a Hitachi S4500 SEM after sputter coating the sample with 3 nm of gold-palladium in a Denton Desk III TSC sputter coater.

Models

Estimates of the persistence lengths of nanofibers of **1** and **2** were obtained from AFM images of unpatterned nanofibers following a method similar to that reported by Frontali et al.[29-31] and Mücke et al.[32] Briefly, the contour of individual nanofibers were traced using ImageJ imaging software (National Institutes of Health) and saved as sets of XY coordinates. Using custom functions written and run in Microcal™ Origin® 6.0, the traces were smoothed and split into multiple sets of varying segment length *s*. For each segment set, the mean-square bending angle $\langle\Theta^2\rangle$ and the mean-square end-to-end distance $\langle R^2\rangle$ were computed. The values of $\langle\Theta^2\rangle$ and $\langle R^2\rangle$ were each fit as functions of *s* to derive values for the persistence length λ:

$$\left\langle \Theta^2(s) \right\rangle = s/\lambda \tag{6}$$

$$\left\langle R^2(s) \right\rangle = 4\lambda s\left(1 - \frac{2\lambda}{s}\left(1 - e^{-s/2\lambda}\right)\right) \tag{7}$$

The persistence length can also be related to the Young's modulus *E* by the equation:[42]

$$EI = k_B T\lambda \tag{8}$$

where *I* is the area moment of inertia calculated from AFM measurements of the nanofiber diameter. This model assumes that the nanofibers are isolated and energetically equilibrated on a two-dimensional solid support. Bundling of multiple nanofibers reduces curvature and increases the apparent stiffness. If the nanofibers are not equilibrated, the apparent value of λ depends on the adsorption mechanism. Strong binding to the substrate tends to decrease λ while shearing by the drying front can increase it.

Polarized IR spectroscopy was used to measure the degree of alignment of the nanofibers patterned by SASE. The orientation of a transition dipole moment (TDM), *M*, of a single molecular vibration may be described with respect to a fixed space coordinate system (*x*, *y*,

z) by the three Euler angles (θ, φ, ψ) and the tilt angle (α) of the TDM relative to the nanofiber long axis (see supporting information). The direction cosines K_i ($i = x, y, z$) of the TDM averaged over all molecules are calculated from the IR absorption intensities.[43] The function of K_i with respect to α, θ, φ, and ψ is determined by straightforward geometric arguments as shown by Zbinden.[44] The patterned nanofibers can be thought of as a biaxially oriented film where the nanofibers preferentially align perpendicular to the *z* axis and parallel to the *x* axis within the *xy* plane. Stein[45, 46] proposed two orientation parameters, f_θ and f_φ, to describe alignment in biaxially oriented films:

$$f_\theta = \frac{3\left\langle \cos^2\theta \right\rangle - 1}{2} \tag{1}$$

$$f_\varphi = 2\left\langle \cos^2\varphi \right\rangle - 1 \tag{2}$$

f_θ is equal to the space-averaged second order Legendre polynomial P_2 describing alignment along the *z* axis out of the substrate plane.[47] f_φ can be thought of as a two-dimensional order parameter quantifying the in-plane alignment of directors along the *x* axis and is used here as the primary figure of merit. The orientation parameters cannot be determined exactly from the three polarized spectra alone, but upper and lower bound values of f_φ can be calculated assuming cylindrical symmetry about the nanofiber axis and specific values of α and θ (see supporting information):[48]

$$f_{\varphi,\min} = \frac{K_x - K_y}{K_x + K_y} \tag{3}$$

$$f_{\varphi,\max} = \frac{K_x - K_y}{K_x + K_y - 2K_z} \tag{4}$$

The spectroscopic model assumes that the material is optically isotropic and that variations in reflectance and refractive index with wavelength are negligible,[49, 50] but the calculated values of f_φ are useful as figures of merit by which the effects of different experimental parameters may be compared within the realm of the proposed molecular model.

Selected peaks in the spectra were fit to Lorentzian forms so that the peak areas could be obtained and the quality of alignment between samples could be quantitatively compared. In the amide I region (1700−1620 cm^{-1}), a rigorous deconvolution of each of the non-β-sheet peaks was not attempted, rather, the peak fitting was performed to the extent to which we were able to reliably determine the area of the β-sheet peak at 1630 cm^{-1}. The amide A band (3310 −3270 cm^{-1}) is much less sensitive to secondary structure[51, 52] and even more difficult to deconvolute, so orientation parameters obtained for the amide A band were used only to qualitatively confirm observed trends.

Another method to confirm the observed trends is to derive orientation parameters directly from AFM images. Using high quality images such as those previously reported,[10] individual nanofibers can be traced, and given the length and biaxial orientation angle of enough nanofibers, a value for $\langle\cos^2\varphi\rangle$ may be calculated. This analysis was performed for PAs **1** and

2 aligned in channels of 278 and 416 nm periodicity, using a total image area of 2 μm^2 for each case.

Results and Discussion

Analysis of AFM images such as those shown in Figure 2a of unpatterned nanofibers yields estimates of their persistence lengths λ as listed in Table 1. Both PAs have apparent values of λ longer than the width of the confining channels used in this study. But while nanofibers of **1** display a value of λ on the order of 2.0 μm corresponding to a Young's modulus of 62 MPa, nanofibers of **2** have an apparent λ of 11 μm and are four or five times stiffer than **1**. This analysis works best using fiber contour lengths in the range of 0.5 to 30 times λ,[29, 30] but nanofibers of **2** with that length are experimentally difficult to find and image. Still, the estimates obtained here match up well with qualitative observations.

Polarized IR spectroscopic measurements were used to gauge the effect of different factors on the alignment of PA nanofibers patterned by SASE. A figure of merit was derived based on the previous finding that peptide segments in these molecules assemble into β-sheet "fins" oriented mostly parallel to the long axis of the fiber.[35, 36, 51, 52] In such a structure, the transition dipole moments (TDM) of both the C=O and N-H stretching bands that comprise the bulk of the amide I β-sheet and amide A peaks, respectively, would orient mostly parallel to the fiber and thus absorb more strongly as the polarization of the incident beam is rotated parallel to the fiber alignment direction. Figure 2c shows polarized transmission FTIR spectra of SASE patterned samples of **1** and **2** exhibiting significant degrees of alignment in capillaries of 416 nm period. As the polarization of the incident beam is rotated from 0° to 90° relative to the fiber alignment direction, the intensities of the amide I β-sheet (1629 cm^{-1}), amide A (3292 cm^{-1}), and CH_2 symmetric stretch (2849 cm^{-1}) peaks all decreased relative to the intensity of the peak at 1660 cm^{-1} which is a convolution of the amide I random coil (~1670 cm^{-1}), β-turn (~1680 cm^{-1}), or α-helix bands (~1650 cm^{-1}). In the cases where the alignment effect is the strongest, the amide II (1544 cm^{-1}) and CH_2 antisymmetric stretch (2920 cm^{-1}) peaks whose TDMs are thought to be oriented more normal to the fiber axis are observed to increase in intensity relative to the peak at 1660 cm^{-1}. The difference between the 0° and 90° polarized spectra is less pronounced for **2** than for **1**, indicating less alignment of the nanofibers. Structurally, the β-sheet character of **2** appears to be greater than for **1**.

Figure 3 shows PM-IRRAS spectra of nanofibers of **1** and **2** patterned in grating channels of 416 nm period. The intensity of the β-sheet peak in this case arises in part because the tilt of the TDM of the parallel β-sheet amide I vibration out of the β-sheet plane.[38, 53] Disorder or twist in the β-sheet arrangement also contribute to this signal. These spectra are consistent with previously reported data on nanofiber monolayers[36] except that the random coil peak is shorter than is observed for drop cast films, making the peak at 1630 cm^{-1} seem more intense. The slower evaporation rate during patterning may lead to greater β-sheet character and less random coil structure. This possibility is notable because changes to the molecular structure of the nanofiber may affect its mechanical properties and bioactivity.

The upper and lower bound values of the nanofiber orientation parameter f_φ as affected by the nature of the PA molecule and channel size are plotted in Figure 4 for selected vibration bands. Based on the β-sheet amide I vibration, fibers of **1** align well in confining channels of 833 nm, 416 nm and 278 nm period, with values of f_φ approaching 0.4 for the amide I and amide A bands. This is equivalent to having 40% of the nanofibers perfectly aligned along the *x* axis with the remainder oriented randomly in the *xy* plane. The $\nu_s(CH_2)$ band also gives sizable values of f_φ around 0.3. Nanofibers of **2** do not align as well as those of **1**, but do show some degree of order, yielding values of $f_\varphi > 0.14$ within channels of 416 nm period and a maximum of 30% alignment of the nanofibers. In addition, values for f_φ obtained by AFM image analysis

and listed in Table 2 are consistent with and sometimes exceed those calculated from the spectroscopic data. Compared to IR spectroscopy, this technique for quantifying alignment is inefficient for analyzing large areas and neglects nanofibers buried beneath the surface layer, but the image analysis helps to validate the spectroscopic model and confirm the observed trends.

Nanofibers of PA **2** have a longer persistence length λ than nanofibers of **1**, yet their alignment by SASE is not as good, contrary to what one would normally expect for alignment of one-dimensional objects in microchannels. Stiff mesogens energetically favor more ordered configurations than flexible mesogens,[54, 55] so one might think that nanofibers of **2**, not **1**, should align better. However, we believe in this case that nanofiber assembly begins before the stamp is able to contact the substrate and establish the confining channels, and alignment occurs not by rotation of whole ca. 10 μm long structures but by cutting the nanofibers into shorter segments, then reorienting and connecting multiple segments within a channel. The value of λ becomes almost moot if the nanofiber is broken into smaller segments. What λ may be indicative of is a greater amount of energy needed to cleave a nanofiber of **2**. While PA **2** is a larger molecule than **1**, a 10 % increase in the nanofiber diameter alone would only predict a 46 % increase in λ. More hydrophobic residues and greater β-sheet character in **2** as observed in the IR spectra likely contribute to a stronger nanofiber. Nanofibers that resist breaking cannot be aligned and instead get compacted into a disordered residual layer that coats the substrate under and between the channels.

Without ultrasonication there is effectively no alignment of nanofibers of **2**, whereas inclusion of the ultrasonication step during patterning appears to have a minimal impact on the degree of order in nanofibers of **1**. This observation is consistent with the hypothesis proposed above that alignment of supramolecular fibers requires the possibility of their rupture into shorter objects. By analogy ultrasonication can erase the mechanical history of actin gels,[56] demonstrating that it aids in breaking and reorienting supramolecular assemblies. Without such aid, nanofibers of **2** readily become kinetically trapped in entangled networks. In contrast, PA **1** is more water soluble which would imply that the inter- and intra-fiber attractive forces are weaker in aqueous media, so nanofibers of **1** are easier to cleave, rotate, and align without the aid of ultrasonication.

Ultrasonication can speed up reorganization of the nanofibers, but it cannot force them to align more than is energetically favorable. The insignificant difference with and without the extra patterning step may mean that nanofibers of **1** are already near their optimal degree of alignment under the conditions studied. However, there is a chance that nanofibers of **2** have yet to reach equilibrium and alignment may be improved by changing the solvent or adjusting the power and duration of the ultrasonication step. Conversely, dispersing **1** in a poorer solvent may hinder alignment without the aid of ultrasonication. This option is interesting because tuning the ultrasonication procedure may allow us to vary the order parameter controllably and across a continuous range of values while keeping the other properties of the nanofiber patterns constant. The ability to do so is useful for subsequent experiments on aligned nanofibers because substrates of non-aligned, patterned nanofibers could be made as control samples for the topology of the pattern. If the alignment is optimized and the scattering contrast in the material increased, the aligned samples could be suitable also for study by x-ray diffraction.

Spectral data show no significant difference in alignment between nanofibers of **1** aligned in any of the three channel widths. Conversely, spectral data of **2** show the best alignment of the nanofibers in the 416 nm period channels, but almost negligible alignment in the smaller channels. This observation is corroborated by AFM images[10] and suggests a lower bound to the length scale in which the supramolecular assemblies prefer to align under confinement while yet having the mobility to do so. PA **2** is more hydrophobic than **1** and may thus interact

more strongly with the PDMS surface of the stamp, hindering the ability of nanofibers of **2** to reorient at high degrees of confinement. The alignment in the 833 nm channels appears to be less than in the 416 nm channels, although not to a significant degree. The order parameter is expected to drop continuously as the size of the channels is increased further. However, this point cannot be definitively proven within the range of channel widths investigated here. The fact that alignment of both **1** and **2** can be observed within channels approaching 833 nm in period and *ca*. 700 nm in width suggests that the method may be effective even for micron scale channels. Achieving alignment in larger channels is desirable because the pattern masters can then be made by photolithography rather than electron-beam or interference lithography.

The values listed in Table 1 for λ assume that the surface adsorbed nanofibers are isolated and energetically equilibrated. Shearing by the drying front would increase the apparent persistence length whereas strong binding to the substrate would decrease it. Both effects are lessened by slow evaporation rates and the use of silicon subtrates with clean native oxide surfaces of partial negative charge that should repel the negatively charged PA molecules. Nanofiber bundling is another factor that can increase the apparent value of λ, but this effect is difficult to mitigate because diluting the PA solution shortens nanofibers in addition to dispersing them. Thus we believe that while the values of λ in Table 1 may overestimate the actual values of single nanofibers, they still reflect differences among PA nanofibers in gels or concentrated solutions.

Conclusions

IR spectroscopic data demonstrate the possibility of orienting supramolecular nanofibers over macroscopic length scales using sonication assisted solution embossing. Measurements of persistence length also suggest that supramolecular nanofibers with greater capacity to fragment and reassemble through secondary bonds under ultrasonication can be more easily patterned and aligned using the technique investigated. Peptide amphiphile nanofibers were aligned within microchannels approaching ca. 700 nm in width, suggesting that this technique might be effective up to the micron length scale where patterned masters could be easily fabricated by photolithography.

Supplementary Material

Refer to Web version on PubMed Central for supplementary material.

Acknowledgements

This work was supported by the U.S. Department of Energy Grant DEFG02-00ER45810 and by the National Institutes of Health grants 5R01EB003806 and 5R01DE015920. AMH is grateful for support received from the National Science Foundation Graduate Research Fellowship Program and the National Defense Science and Engineering Graduate Fellowship Program. We thank the NUANCE Center facilities for the use of the AFM, SEM, and FTIR/PMIRRAS spectrometer, and the Materials Research, Processing, and Crystal Growth Facility (MRPCGF) for the use of the electron-beam evaporator and RIE at Northwestern University. The authors are grateful to Dorothea Grieshaber for early experimental help and to Dr. Krista L. Niece for materials synthesis and useful comments on the manuscript.

References

1. Lehn JM. Angew. Chem. Int. Ed 1988;27:89.
2. Philp D, Stoddart JF. Angew. Chem. Int. Ed 1996;35:1155.
3. Reinhoudt DN, Crego-Calama M. Science 2002;295:2403. [PubMed: 11923525]
4. Stupp SI, LeBonheur V, Walker K, Li LS, Huggins KE, Keser M, Amstutz A. Science 1997;276:384. [PubMed: 9103190]
5. Hamley IW. Angew. Chem. Int. Ed 2003;42:1692.

6. Hoeben FJM, Jonkheijm P, Meijer EW, Schenning A. Chem. Rev 2005;105:1491. [PubMed: 15826018]
7. Whitesides GM, Grzybowski B. Science 2002;295:2418. [PubMed: 11923529]
8. Alivisatos AP, Barbara PF, Castleman AW, Chang J, Dixon DA, Klein ML, McLendon GL, Miller JS, Ratner MA, Rossky PJ, Stupp SI, Thompson ME. Adv. Mater 1998;10:1297.
9. Hartgerink JD, Zubarev ER, Stupp SI. Curr. Opin. Solid State Mater. Sci 2001;5:355.
10. Hung AM, Stupp SI. Nano Lett 2007;7:1165. [PubMed: 17447823]
11. Jiang HZ, Stupp SI. Langmuir 2005;21:5242. [PubMed: 15924443]
12. Kim JS, McHugh SK, Swager TM. Macromolecules 1999;32:1500.
13. Messmore BW, Hulvat JF, Sone ED, Stupp SI. J. Amer. Chem. Soc 2004;126:14452. [PubMed: 15521765]
14. Sardone L, Palermo V, Devaux E, Credgington D, De Loos M, Marletta G, Cacialli F, Van Esch J, Samori P. Adv. Mater 2006;18:1276.
15. Zhao Y, Fang JY. Langmuir 2006;22:1891. [PubMed: 16460124]
16. Kato T, Kutsuna T, Yabuuchi K, Mizoshita N. Langmuir 2002;18:7086.
17. Hartgerink JD, Beniash E, Stupp SI. Science 2001;294:1684. [PubMed: 11721046]
18. Silva GA, Czeisler C, Niece KL, Beniash E, Harrington DA, Kessler JA, Stupp SI. Science 2004;303:1352. [PubMed: 14739465]
19. Rajangam K, Behanna HA, Hui MJ, Han XQ, Hulvat JF, Lomasney JW, Stupp SI. Nano Lett 2006;6:2086. [PubMed: 16968030]
20. Tysseling-Mattiace VM, Sahni V, Niece KL, Birch D, Czeisler C, Fehlings MG, Stupp SI, Kessler JA. J. Neurosci 2008;28:3814. [PubMed: 18385339]
21. Beniash E, Hartgerink JD, Storrie H, Stendahl JC, Stupp SI. Acta Biomater 2005;1:387. [PubMed: 16701820]
22. Kas J, Strey H, Sackmann E. Nature 1994;368:226. [PubMed: 8145821]
23. Hirst LS, Parker ER, Abu-Samah Z, Li Y, Pynn R, MacDonald NC, Safinya CR. Langmuir 2005;21:3910. [PubMed: 15835954]
24. Bouxsein NF, Hirst LS, Li YL, Safinya CR, Abu Samah Z, MacDonald NC, Pynn R. Appl. Phys. Lett 2004;85:5775.
25. Jonkheijm P, Hoeben FJM, Kleppinger R, van Herrikhuyzen J, Schenning A, Meijer EW. J. Amer. Chem. Soc 2003;125:15941. [PubMed: 14677986]
26. Kasas S, Dietler G. Curr. Nanosci 2007;3:85.
27. Ezrahi S, Tuval E, Aserin A. Adv. Colloid Interfac 2006;128:77.
28. Gittes F, Mickey B, Nettleton J, Howard J. J. Cell Biol 1993;120:923. [PubMed: 8432732]
29. Bettini A, Pozzan MR, Valdevit E, Frontali C. Biopolymers 1980;19:1689.
30. Frontali C. Biopolymers 1988;27:1329. [PubMed: 2851336]
31. Frontali C, Dore E, Ferrauto A, Gratton E, Bettini A, Pozzan MR, Valdevit E. Biopolymers 1979;18:1353. [PubMed: 465647]
32. Mucke N, Kreplak L, Kirmse R, Wedig T, Herrmann H, Aebi U, Langowski J. J. Mol. Biol 2004;335:1241. [PubMed: 14729340]
33. Niece KL, Hartgerink JD, Donners J, Stupp SI. J. Amer. Chem. Soc 2003;125:7146. [PubMed: 12797766]
34. Stendahl JC, Rao MS, Guler MO, Stupp SI. Adv. Funct. Mater 2006;16(4):499–508.
35. Paramonov SE, Jun HW, Hartgerink JD. J. Amer. Chem. Soc 2006;128:7291. [PubMed: 16734483]
36. Jiang HZ, Guler MO, Stupp SI. Soft Matter 2007;3:454.
37. Kim HS, Hartgerink JD, Ghadiri MR. J. Amer. Chem. Soc 1998;120:4417.
38. Marsh D. Biophys. J 1997;72:2710. [PubMed: 9168046]
39. Wang J, Chen XY, Clarke ML, Chen Z. J. Phys. Chem. B 2006;110:5017. [PubMed: 16526745]
40. Buffeteau T, Desbat B, Turlet JM. Polarization Modulation Ft-Ir Spectroscopy of Surfaces and Ultra-Thin Films - Experimental Procedure and Quantitative-Analysis. Applied Spectroscopy 1991;45(3): 380–389.

41. Hartgerink JD, Beniash E, Stupp SI. Proc. Natl. Acad. Sci. U.S.A 2002;99:5133. [PubMed: 11929981]
42. Landau, LD.; Lifshitz, EM. Statistical Physics, Part 1. Vol. 3rd ed.. Pergamon Press; New York: 1980.
43. Thulstrup, EW.; Michl, J. Elementary Polarization Spectroscopy. VCH; New York: 1989.
44. Zbinden, R. Infrared Spectroscopy of High Polymers. Academic Press; New York: 1964.
45. Stein RS. J. Polym. Sci 1958;31:327.
46. Stein RS. J. Polym. Sci 1958;31:335.
47. Onsager L. Ann. N.Y. Acad. Sci 1949;51:627.
48. Pelletier I, Laurin I, Buffeteau T, Pezolet M. J. Phys. Chem. B 2004;108:7162.
49. Axelsen PH, Citra MJ. Prog. Biophys. Mol. Biol 1996;66:227. [PubMed: 9284452]
50. Parikh AN, Allara DL. J. Chem. Phys 1992;96:927.
51. Barth A, Zscherp C. Q. Rev. Biophys 2002;35:369. [PubMed: 12621861]
52. Krimm S, Bandekar J. Adv. Protein Chem 1986;38:181. [PubMed: 3541539]
53. Miyazawa T. J. Chem. Phys 1960;32:1647.
54. Khokhlov AR, Semenov AN. Physica A 1982;112:605.
55. Wang, XJ.; Zhou, QF. Liquid Crystalline Polymers. World Scientific; River Edge, NJ: 2004.
56. Helfer E, Panine P, Carlier MF, Davidson P. Biophys. J 2005;89:543. [PubMed: 15863487]

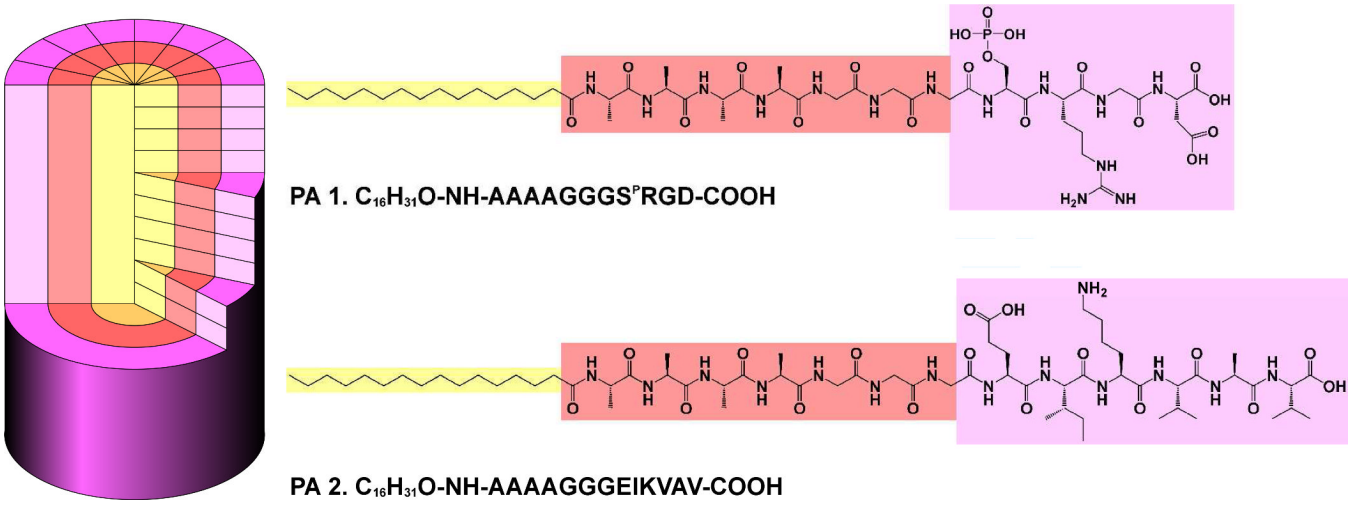

Figure 1.
Chemical structures of PA molecules **1** and **2**

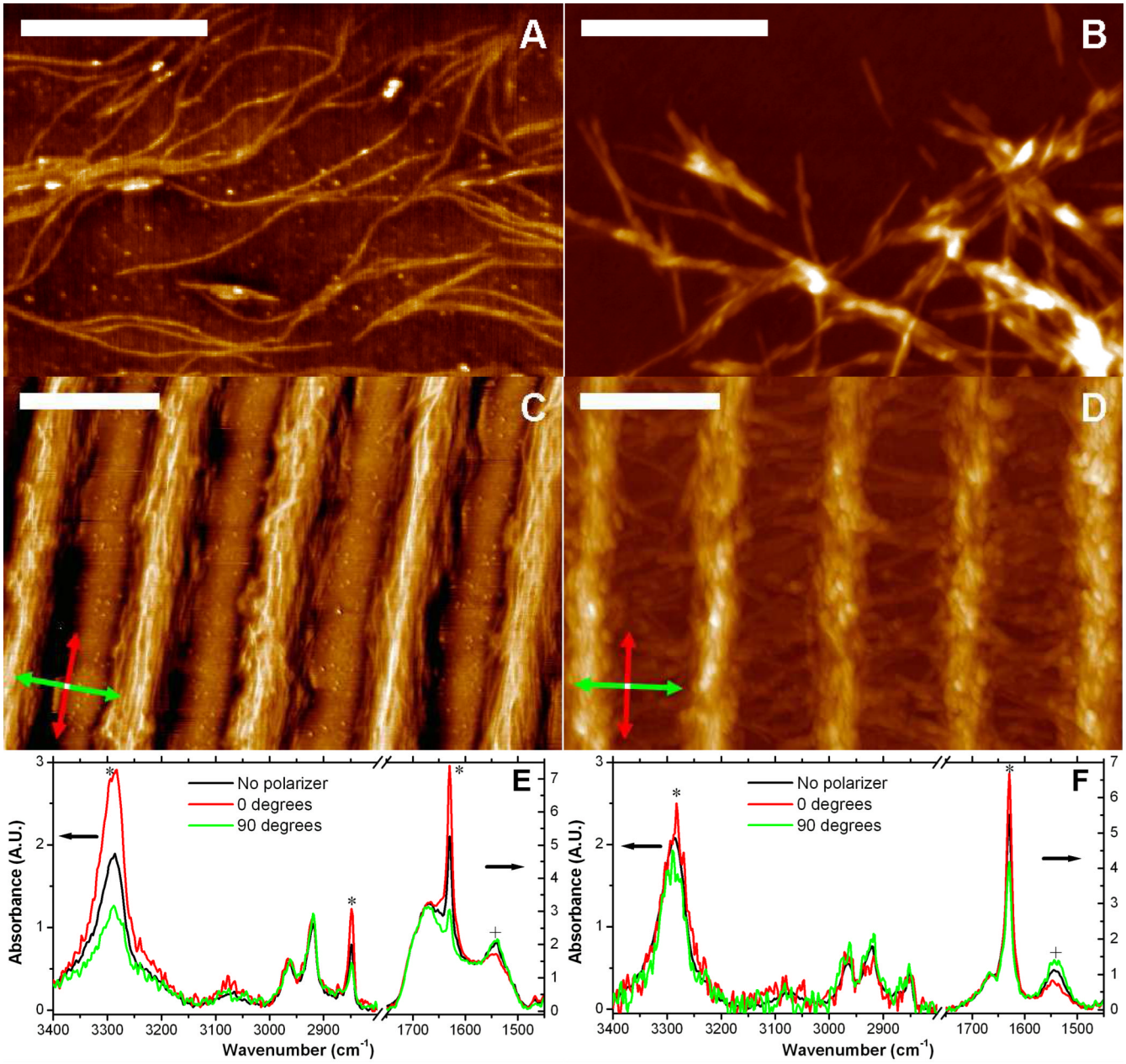

Figure 2.

AFM images of nanofibers of (**a**, **c**; phase contrast) PA **1** and (**b**, **d**; height contrast) PA **2** both (**a**, **b**) unpatterned and (**c**, **d**) aligned by SASE in gratings of 416 nm period (2400 lines/mm). Unbroken, misaligned nanofibers can be seen between the tracks in **d**. Scale bars are 500 nm. Polarized transmission FTIR spectra of patterned nanofibers of (**e**) **1** and (**f**) **2** show their alignment in the 416 nm period gratings. Spectra are normalized to the intensity of the residual silane $\delta_s(CH_3)$ symmetric deformation at 1261 cm^{-1}. Transition dipole moments oriented parallel (*) and perpendicular (+) to the fiber structure can be readily identified as the incident polarization is rotated from 0° (red) to 90° (green) relative to the alignment direction.

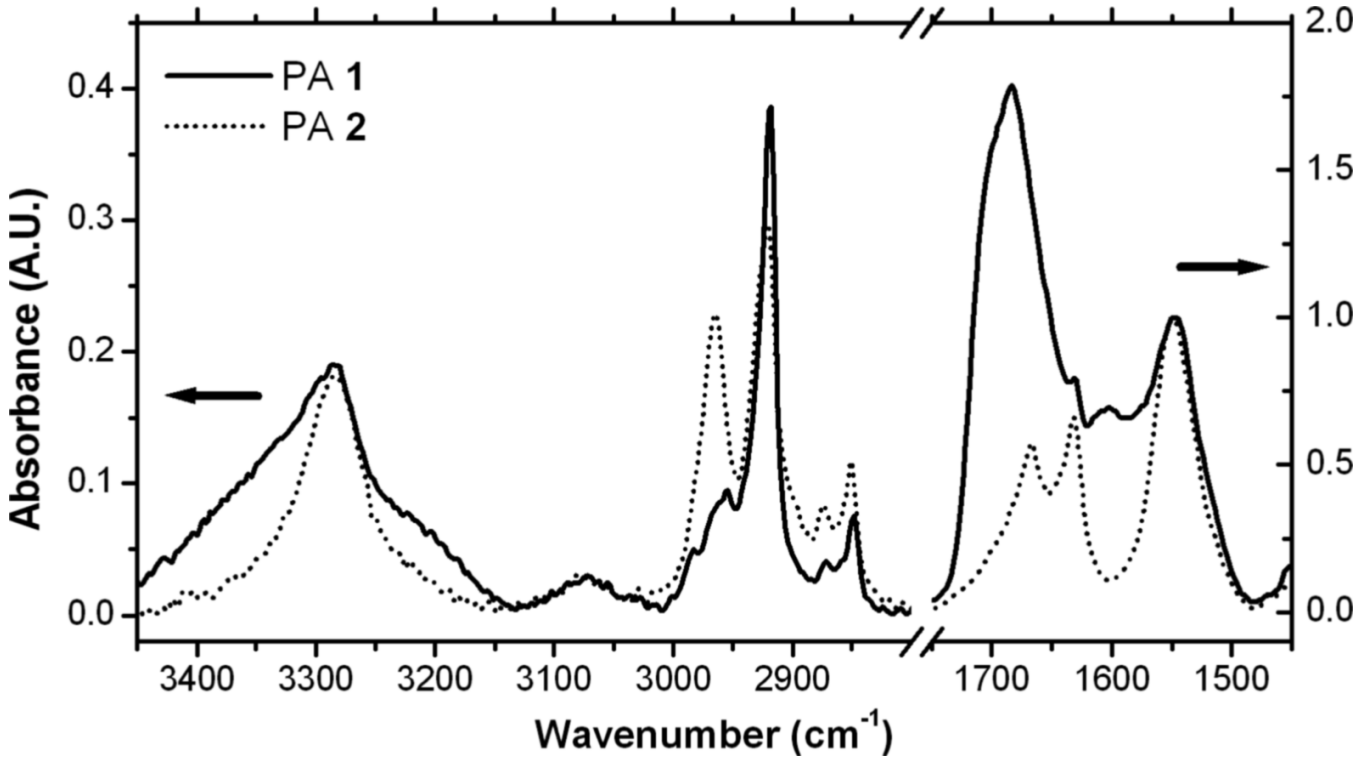

Figure 3.
PM-IRRAS spectra of PAs **1** and **2** patterned in gratings of 416 nm period.

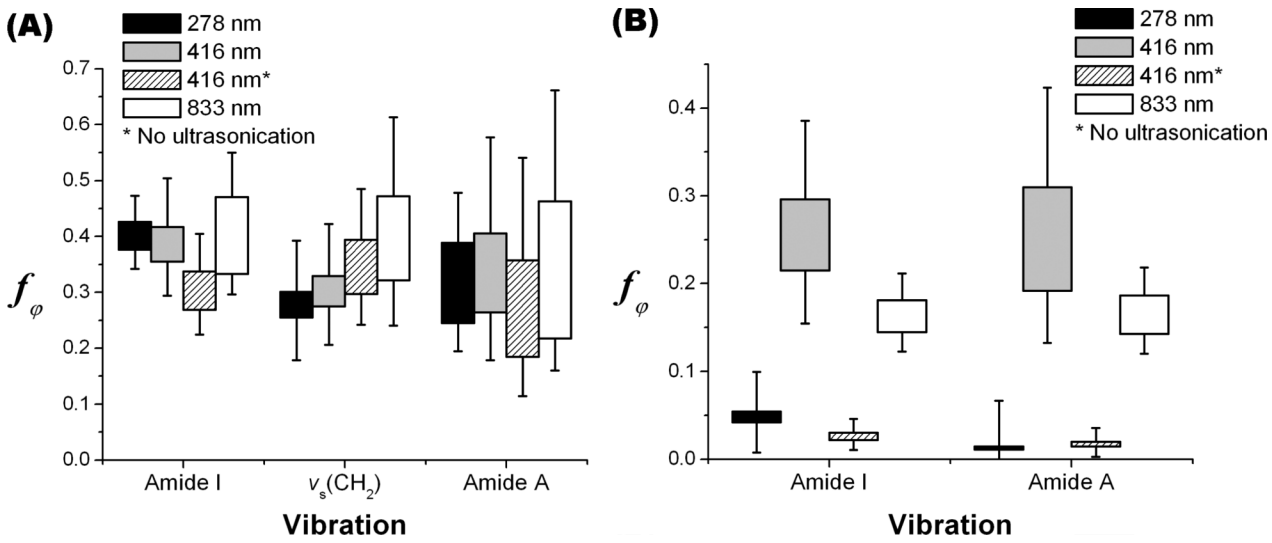

Figure 4.

Upper and lower bound values of the orientational order parameter f_φ calculated from selected IR bands for nanofibers of (**a**) PA **1** and (**b**) PA **2** aligned in grating channels of different periodicities.

Table 1

Persistence lengths and stiffnesses of PA nanofibers from AFM image analysis

PA	$\lambda_{<\Theta^2>}$ (μm)	$\lambda_{<R^2>}$ (μm)	Trace length (μm)	Counts	Nanofiber diameter (nm)	*E* (MPa)
1	1.97 ± 0.35	2.00 ± 0.38	1.88 ± 0.25	43	7.2	62
2	11.0 ± 2.2	11.0 ± 2.0	2.27 ± 0.32	39	7.6	280

The persistence lengths $\lambda_{<\Theta^2>}$ and $\lambda_{<R^2>}$ were estimated from the experimental angle and end-to-end distance distributions, respectively. An average of the two values was used to calculate a value for the Young's modulus *E*.

Table 2

Values of f_{φ} obtained by analysis of AFM images.

PA	Channel period (nm)	f_{φ}
1	278	0.75
	416	0.50
2	278	0.04
	416	0.27
	416*	0.05

* No ultrasonication